DOI: 10.23968/2500-0055-2025-10-4-100-111

ENGINEERING METHOD FOR DETERMINING THERMAL STRESSES DURING CONSTRUCTION OF FOUNDATION SLABS CONSIDERING FOUNDATION SOIL COMPLIANCE

Vasilina Sergeevna Tyurina, Anton Sergeevich Chepurnenko*, Vladimir Feliksovich Akopyan

Don State Technical University, Rostov-on-Don, Russia

*Corresponding author's email: anton_chepurnenk@mail.ru

Abstract

Introduction. Massive monolithic foundation slabs are prone to early-age cracking caused by the exothermic heat of hydration of concrete. Selecting optimal strategies to address this issue can be achieved through computer-based simulations. **Purpose of the study**. The study is aimed at developing a simplified finite element model to determine the stress–strain state of foundation slabs during construction while accounting for foundation soil compliance, and validating this model against existing experimental data as well as results reported by other authors. In the course of the study, the following **methods** were used: finite element modeling with plate finite elements in the MATLAB environment, employing software developed by the authors that reduces the three-dimensional problem of determining the stress–strain state to a two-dimensional formulation. The foundation bed was modeled using the Pasternak model with two foundation moduli. The **results** show that the proposed solution is in good agreement with the numerical modeling data obtained by other researchers in a three-dimensional setting. Satisfactory agreement with the experimental results was also achieved. A study was conducted to assess the influence of the reinforcement ratio and the coefficient of linear thermal expansion of concrete on the stress–strain state.

Keywords: massive reinforced concrete structures; foundation slab; cracking; thermal stresses; finite element method; foundation modulus.

Introduction

The increasing height of constructed buildings makes research aimed at improving foundation design and construction technology particularly relevant, with the objective of enhancing structural reliability and reducing costs. Widely used flat monolithic reinforced concrete foundation slabs typically have a thickness of 50–200 cm or more (Bushmanova et al., 2017). In most cases, such foundation slabs with a thickness exceeding 70 cm fall into the category of massive structures (Johansson and Heinegård, 2020). In massive reinforced concrete foundation slabs, the heat released during cement hardening causes non-uniform temperature rise across the slab thickness (Kuriakose et al., 2016). Differential thermal strains in combination with shrinkage deformations can generate significant tensile stresses leading to cracking (Chuc et al., 2018; Klemczak and Knoppik-Wróbel, 2011; Korotchenko et al., 2016). Early-age cracking in massive reinforced concrete structures may require substantial additional costs, and in some cases may render the structure unfit for service (Safiuddin et al., 2018). It also adversely affects durability and long-term structural performance under loading (Slowik et al., 2008). Therefore, for such structures, special measures must be implemented to minimize the influence of thermal stresses associated with concrete exothermy during hardening (Nama et al., 2015).

Selecting optimal mix-design and technological parameters for casting monolithic foundation slabs can also be based on numerical modeling results (Buffo-Lacarrière et al., 2011; Havlásek et al., 2017; Wang et al., 2020).

At present, the finite element method serves as the main tool for analyzing temperature fields and thermal stresses in massive monolithic foundation slabs during construction (Liu and Schindler, 2020; Mathern and Yang, 2021).

The analysis of temperature fields and thermal stresses during the construction of massive monolithic foundation slabs is typically carried out in a three-dimensional setting using solid finite elements (FE) for both the concrete and the foundation soil (Cajka et al., 2020). This approach requires substantial computational resources, which makes it difficult to explore a large number of options when choosing optimal casting parameters.

An earlier study (Chepurnenko et al., 2022b) proposed a simplified method for determining thermal stresses during the construction of massive monolithic foundation slabs resting on a completely rigid base. In addition to assuming that the base is non-deformable, the method also considers identical reinforcement in the *x* and *y* axes and uses

For citations: Tyurina, V. S., Chepurnenko, A. S., Akopyan, V. F. (2025). Engineering method for determining thermal stresses during construction of foundation slabs considering foundation soil compliance. Architecture and Engineering, No 4 (10), pp. 100–111. DOI: 10.23968/2500-0055-2025-10-4-100-111.

the plane-sections hypothesis, which reduces the three-dimensional stress–strain analysis to a one-dimensional problem.

In (Chepurnenko et al., 2024), a resolving equation was derived to determine the stress–strain state of a foundation slab during construction while accounting for foundation slab compliance. The Pasternak elastic foundation model was adopted for the soil. The foundation slab was considered as plain concrete, without accounting for reinforcement. Moreover, a finite-difference method was proposed to solve the resulting equation, which leads to relatively complex approximations of boundary conditions.

The objective of this study is to further develop the approaches proposed by Chepurnenko et al. (2024). The method presented in this paper allows the reinforcement of the slab to differ in the *x* and *y* axes. The idea is to reduce the three-dimensional thermal stress analysis to a two-dimensional problem based on the assumption of a linear distribution of strains through the slab thickness and the use of plate finite elements instead of solid FE.

Materials and Methods

In this study, reinforced concrete foundation slabs with orthogonal reinforcement are considered (Fig. 1). To reduce the dimensionality of the problem, the hypothesis of a linear strain distribution through the slab thickness (straight-normal hypothesis) is used. This hypothesis is valid for thin plates in which the ratio of thickness *h* to the smallest plan dimension *a* does not exceed one fifth (Petrov, 2018). Despite their considerable thickness, which may reach 2.5 m or more, foundation slabs also have significant plan dimensions. Therefore, the ratio *h*/*a* generally falls within the specified limits, and the use of the straight-normal hypothesis can be considered justified for this problem. When these limits are exceeded, one may employ, for example, the hypotheses presented in (Gatiev et al., 2023).

Based on the straight-normal hypothesis, the total concrete strains $\varepsilon_{bx}, \varepsilon_{by}, \gamma_{bxy}$ can be written as follows:

$$\begin{aligned} \varepsilon_{bx} &= \varepsilon_x^0 - z\chi_x; \\ \varepsilon_{by} &= \varepsilon_y^0 - z\chi_y; \\ \gamma_{bxy} &= \gamma^0 - 2z\chi_{xy}, \end{aligned} \quad (1)$$

where ε_x^0, ε_y^0, γ_0 are the strains of the middle plane (taken as the reference surface), $\chi_x = \frac{\partial^2 w}{\partial x^2}$, $\chi_x = \frac{\partial^2 w}{\partial y^2}$, $\chi_{xy} = \frac{\partial^2 w}{\partial x \partial y}$ are the mid-surface curvature changes, w is the slab deflection, and the coordinate is measured from the middle plane.

The strains of the reinforcement in the *i*-th layer are determined from the condition of its combined action with the concrete:

$$\varepsilon_{sx,i} = \varepsilon_x^0 - z_{sx,i}\chi_x;$$

$$\varepsilon_{sy,i} = \varepsilon_y^0 - z_{sy,i}\chi_y. \quad (2)$$

In addition to the hypothesis of linear strain distribution through the slab thickness, a hypothesis on the one-dimensional character of temperature distribution is introduced, i.e., the temperature is assumed to be a function of the coordinate z only. This is confirmed by the results of three-dimensional finite element simulations presented in (Chepurnenko et al., 2022a, 2022b). A deviation from this hypothesis is observed only in a small region near the slab edges. Since the temperature is taken as a function of z only, the concrete modulus of elasticity is also assumed to depend solely on z. The well-known plate theory assumption of the absence of transverse normal stresses is also adopted, meaning that strains and stresses in the z direction are absent in the concrete.

The total concrete strains, from a physical standpoint, represent the sum of the strains caused by stresses σ_{bx}, σ_{by}, and τ_{bxy}, as well as thermal strains and shrinkage strains:

$$\begin{aligned} \varepsilon_{bx} &= \frac{1}{E_b(z)}\left(\sigma_{bx} - \nu\sigma_{by}\right) + \varepsilon_{bf}; \\ \varepsilon_{by} &= \frac{1}{E_b(z)}\left(\sigma_{by} - \nu\sigma_{bx}\right) + \varepsilon_{bf}; \\ \gamma_{bxy} &= \frac{2(1+\nu)}{E_b(z)}\tau_{bxy}, \end{aligned} \quad (3)$$

where $E_b(z)$ is the concrete modulus of elasticity; ν is the Poisson's ratio of concrete, taken as constant; $\varepsilon_{bf} = \alpha\Delta T + \varepsilon_{sh}$ is the sum of the thermal strain and shrinkage strain (α is the coefficient of linear thermal expansion of concrete; ΔT is the temperature change at the point under consideration).

The total strains in the reinforcement consist of elastic and thermal strains:

$$\begin{aligned} \varepsilon_{sx,i} &= \frac{\sigma_{sx,i}}{E_s} + \alpha_s \Delta T_{x,i}; \\ \varepsilon_{sy,i} &= \frac{\sigma_{sy,i}}{E_s} + \alpha_s \Delta T_{y,i}, \end{aligned} \quad (4)$$

where $\sigma_{sx,i}$ and $\sigma_{sy,i}$ are the stresses in the steel reinforcement in the x and y directions, E_s is the elastic modulus of steel, $\Delta T_{x,i}$ and $\Delta T_{y,i}$ are the

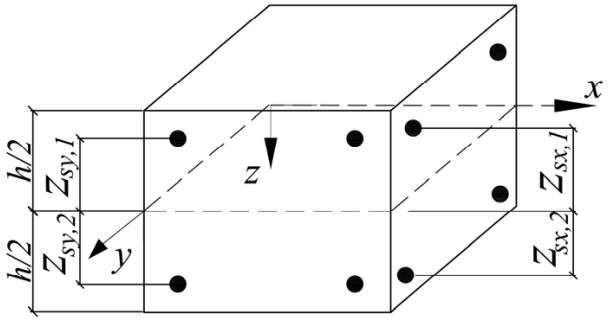

Fig. 1. Slab reinforcement layout

temperature changes in the i-th layer in the x and y directions, and α_s is the coefficient of linear thermal expansion of steel.

The stresses in concrete are expressed from (3) through the strains in the following form:

$$\sigma_{bx} = \frac{E_b(z)}{1-\nu^2}\left(\varepsilon_{bx} + \nu\varepsilon_{by} - (1+\nu)\varepsilon_{bf}\right) =$$

$$= \frac{E_b(z)}{1-\nu^2}\left(\varepsilon_x^0 + \nu\varepsilon_y^0 + z\left(\chi_x + \nu\chi_y\right) - (1+\nu)\varepsilon_{bf}\right);$$

$$\sigma_{by} = \frac{E_b(z)}{1-\nu^2}\left(\varepsilon_{by} + \nu\varepsilon_{bx} - (1+\nu)\varepsilon_{bf}\right) =$$

$$= \frac{E_b(z)}{1-\nu^2}\left(\varepsilon_y^0 + \nu\varepsilon_x^0 + z\left(\chi_y + \nu\chi_x\right) - (1+\nu)\varepsilon_{bf}\right);$$

$$\tau_{bxy} = \frac{E_b(z)}{2(1+\nu)}\gamma_{bxy} = \frac{E_b(z)}{2(1+\nu_b)}\left(\gamma_0 - 2z\chi_{xy}\right). \quad (5)$$

The stresses in the reinforcement are written through the strains as follows:

$$\sigma_{sx,i} = E_s\left(\varepsilon_x^0 - z_{sx,i}\chi_x - \alpha_s\Delta T_{x,i}\right);$$

$$\sigma_{sy,i} = E_s\left(\varepsilon_y^0 - z_{sy,i}\chi_y - \alpha_s\Delta T_{y,i}\right). \quad (6)$$

In the analysis, it is assumed that the slab resists only bending, and that no longitudinal forces N_x, N_y develop, since the soil has a much lower modulus of elasticity compared with concrete and therefore does not restrain the slab from expanding in the x and y directions. The shear forces N_{xy} are also taken equal to zero. The conditions of zero longitudinal forces are written as follows:

$$N_x = \int_{-\frac{h}{2}}^{\frac{h}{2}} \sigma_{bx}dz + \sum_{i=1}^{n_x}\sigma_{sx,i}A_{sx,i} = 0;$$

$$N_y = \int_{-\frac{h}{2}}^{\frac{h}{2}} \sigma_{by}dz + \sum_{i=1}^{n_y}\sigma_{sy,i}A_{sy,i} = 0, \quad (7)$$

where n_x and n_y are the numbers of reinforcement layers in the x and y directions, $A_{sx,i}$ and $A_{sy,i}$ are the cross-sectional areas of the reinforcement in the i-th layer per running meter of the slab length.

Substituting (5) and (6) into the first equation of (7) yields the following:

$$\left(B_{b1} + B_{sx}\right)\varepsilon_x^0 + B_{b2}\varepsilon_y^0 - \left(C_{b1} + C_{sx}\right)\chi_x - C_{b2}\chi_y =$$
$$= N_{bf} + N_{sfx}, \quad (8)$$

where

$$B_{b1} = \frac{1}{1-\nu_b^2}\int_{-h/2}^{h/2} E_b(z)dz;$$

$$B_{b2} = \nu B_{b1},\ C_{b1} = \frac{1}{1-\nu_b^2}\int_{-h/2}^{h/2} E_b(z)zdz;$$

$$C_{b2} = \nu C_{b1};\ B_{sx} = E_s\sum_{i=1}^{n_x}A_{sx,i};\ C_{sx} = \sum_{i=1}^{n_x}A_{sx,i}z_{sx,i};$$

$$N_{bf} = \frac{1}{1-\nu}\int_{-h/2}^{h/2} E_b(z)\varepsilon_{bf}dz;$$

$$N_{sfx} = \alpha_s E_s\sum_{i=1}^{n_x}A_{sx,i}\Delta T_{x,i}.$$

Similarly, the condition $N_y = 0$ gives:

$$\left(B_{b1} + B_{sy}\right)\varepsilon_y^0 + B_{b2}\varepsilon_x^0 - \left(C_{b1} + C_{sy}\right)\chi_y - C_{b2}\chi_x =$$
$$= N_{bf} + N_{sfy}, \quad (9)$$

where

$$B_{sy} = E_s\sum_{i=1}^{n_y}A_{sy,i};\ C_{sy} = \sum_{i=1}^{n_y}A_{sy,i}z_{sy,i};$$

$$N_{sfy} = \alpha_s E_s\sum_{i=1}^{n_y}A_{sy,i}\Delta T_{y,i}.$$

The strains ε_x^0 and ε_y^0 can be expressed from (8) and (9) through changes in curvatures as follows:

$$\begin{Bmatrix}\varepsilon_x^0\\ \varepsilon_y^0\end{Bmatrix} = [A]\begin{Bmatrix}\chi_x\\ \chi_y\end{Bmatrix} + \begin{bmatrix}B_{b1}+B_{sx} & B_{b2}\\ B_{b2} & B_{b1}+B_{sy}\end{bmatrix}^{-1}\times$$
$$\times\begin{Bmatrix}N_{fx}\\ N_{fy}\end{Bmatrix}, \quad (10)$$

where

$$[A] = \begin{bmatrix}B_{b1}+B_{sx} & B_{b2}\\ B_{b2} & B_{b1}+B_{sy}\end{bmatrix}^{-1}\cdot\begin{bmatrix}C_{b1}+C_{sx} & C_{b2}\\ C_{b2} & C_{b1}+C_{sy}\end{bmatrix};$$
$$N_{fx} = N_{bf} + N_{sfx};\ N_{fy} = N_{bf} + N_{sfy}.$$

The bending moments M_x and M_y are determined as follows:

$$M_x = \int_{-\frac{h}{2}}^{\frac{h}{2}} \sigma_{bx}zdz + \sum_{i=1}^{n_x}\sigma_{sx,i}A_{sx,i}z_{sx,i};$$

$$M_y = \int_{-\frac{h}{2}}^{\frac{h}{2}} \sigma_{by}zdz + \sum_{i=1}^{n_y}\sigma_{sy,i}A_{sy,i}z_{sy,i}. \quad (11)$$

Substituting (5) and (6) into (11) yields:

$$\begin{Bmatrix}M_x\\ M_y\end{Bmatrix} = \begin{bmatrix}C_{b1}+C_{sx} & C_{b2}\\ C_{b2} & C_{b1}+C_{sy}\end{bmatrix}\times$$
$$\times\begin{Bmatrix}\varepsilon_x^0\\ \varepsilon_y^0\end{Bmatrix} - \begin{bmatrix}D_{b1}+D_{sx} & D_{b2}\\ D_{b2} & D_{b1}+D_{sy}\end{bmatrix}\times$$
$$\times\begin{Bmatrix}\chi_x\\ \chi_y\end{Bmatrix} - \begin{Bmatrix}M_{bf}+M_{sfx}\\ M_{bf}+M_{sfy}\end{Bmatrix}, \quad (12)$$

where

$$D_{b1} = \frac{1}{1-\nu_b^2}\int_{-h/2}^{h/2} E_b(z)z^2dz;\ D_{b2} = \nu D_{b1};$$

$$D_{sx} = \sum_{i=1}^{n_x}A_{sx,i}z_{sx,i}^2;\ D_{sy} = \sum_{i=1}^{n_y}A_{sy,i}z_{sy,i}^2;$$

$$M_{sfx} = \alpha_s E_s \sum_{i=1}^{n_x} A_{sx,i} \Delta T_{x,i} z_{sx,i};$$

$$M_{sfy} = \alpha_s E_s \sum_{i=1}^{n_y} A_{sy,i} \Delta T_{y,i} z_{sy,i}.$$

To eliminate the mid-surface strains from (12), expression (10) shall be substituted into (12). As a result, the following relationship between the bending moments and the changes in curvatures can be obtained:

$$\begin{Bmatrix} M_x \\ M_y \end{Bmatrix} = -\begin{bmatrix} D_{11} & D_{12} \\ D_{21} & D_{22} \end{bmatrix} \cdot \begin{Bmatrix} \chi_x \\ \chi_y \end{Bmatrix} - \begin{Bmatrix} M_x^* \\ M_y^* \end{Bmatrix}, \quad (13)$$

where

$$\begin{bmatrix} D_{11} & D_{12} \\ D_{21} & D_{22} \end{bmatrix} =$$

$$= \begin{bmatrix} D_{b1} + D_{sx} & D_{b2} \\ D_{b2} & D_{b1} + D_{sy} \end{bmatrix} - \begin{bmatrix} C_{b1} + C_{sx} & C_{b2} \\ C_{b2} & C_{b1} + C_{sy} \end{bmatrix} [A];$$

$$\begin{Bmatrix} M_x^* \\ M_y^* \end{Bmatrix} = \begin{Bmatrix} M_{bf} + M_{sfx} \\ M_{bf} + M_{sfy} \end{Bmatrix} - \begin{bmatrix} C_{b1} + C_{sx} & C_{b2} \\ C_{b2} & C_{b1} + C_{sy} \end{bmatrix} \times$$

$$\times \begin{bmatrix} B_{b1} + B_{sx} & B_{b2} \\ B_{b2} & B_{b1} + B_{sy} \end{bmatrix}^{-1} \begin{Bmatrix} N_{fx} \\ N_{fy} \end{Bmatrix}.$$

It should be noted that $D_{12} = D_{21}$.

The shear force N_{bxy} is determined as follows:

$$N_{bxy} = \int_{-\frac{h}{2}}^{\frac{h}{2}} \tau_{bxy} dz =$$

$$= \frac{\gamma_0}{2(1+\nu)} \int_{-\frac{h}{2}}^{\frac{h}{2}} E_b(z) dz - \frac{\chi_{xy}}{1+\nu} \int_{-\frac{h}{2}}^{\frac{h}{2}} E_b(z) dz. \quad (14)$$

The mid-surface strain γ_0 from (14) is expressed through the torsional curvature χ_{xy} as follows:

$$\gamma_0 = \frac{2C_{b1}}{B_{b1}} \chi_{xy}. \quad (15)$$

In case of orthogonal reinforcement, the torsional moment M_{xy} is entirely accepted by concrete:

$$M_{xy} = \int_{-\frac{h}{2}}^{\frac{h}{2}} \tau_{bxy} z dz =$$

$$= \frac{\gamma_0}{2(1+\nu)} \int_{-h/2}^{h/2} E_b(z) z dz - \frac{\chi_{xy}}{1+\nu} \int_{-\frac{h}{2}}^{\frac{h}{2}} E_b(z) z^2 dz. \quad (16)$$

Substituting (15) into (16) yields:

$$M_{xy} = -(1-\nu)\left(D_{b1} - \frac{C_{b1}^2}{B_{b1}} \right) \chi_{xy} = -D_{33} \chi_{xy}. \quad (17)$$

Finally, the relationship between the internal moments and the changes in curvatures can be written in the following form:

$$\begin{Bmatrix} M_x \\ M_y \\ M_{xy} \end{Bmatrix} = -[D]\{\kappa\} - \{M^*\}, \quad (18)$$

where

$$[D] = \begin{bmatrix} D_{11} & D_{12} & 0 \\ D_{21} & D_{22} & 0 \\ 0 & 0 & D_{33}/2 \end{bmatrix}, \{\kappa\} = \begin{Bmatrix} \chi_x \\ \chi_y \\ 2\chi_{xy} \end{Bmatrix};$$

$$\{M^*\} = \begin{Bmatrix} M_x^* \\ M_y^* \\ 0 \end{Bmatrix}.$$

The calculation of the stress–strain state is performed using the finite element method. Rectangular plate finite elements are employed (Fig. 2), each node having three degrees of freedom: the deflection w_i and the rotation angle φ_i^x, φ_i^y.

To obtain the stiffness matrix and the load vector, the variational Lagrange principle (principle of minimum total energy) is applied.

The total energy functional Λ represents the difference between the potential strain energy and the work of external forces:

$$\Lambda = \Pi - W. \quad (19)$$

The potential strain energy, taking into account thermal effects and concrete shrinkage, can be written as follows:

$$\Pi = \frac{1}{2} \int_A \{\kappa\}^T [D] \{\kappa\} dA + \int_A \{\kappa\}^T dA \cdot \{M^*\}, \quad (20)$$

where $A = a \cdot b$ is the area of the rectangular plate FE.

The work of external forces W represents the work of the reactive pressure of the elastic base. The Pasternak foundation model with two foundation moduli C_1 and C_2 is adopted (Egorova et al., 2016), in which the reactive pressure p is related to the slab deflection as follows:

$$p = C_1 w - C_2 \left(\frac{\partial^2 w}{\partial x^2} + \frac{\partial^2 w}{\partial y^2} \right) = C_1 w - C_2 \nabla^2 w. \quad (21)$$

For a homogeneous soil mass, the moduli C_1 and C_2 are determined by the following formulas:

$$C_1 = \frac{E_g}{H(1-\nu_g^2)}; \quad (22)$$

$$C_2 = \frac{E_g H}{6(1+\nu_g)}, \quad (23)$$

where H is the thickness of the soil mass, E_g is the Young's modulus of the soil, ν_g is the Poisson's ratio of the soil.

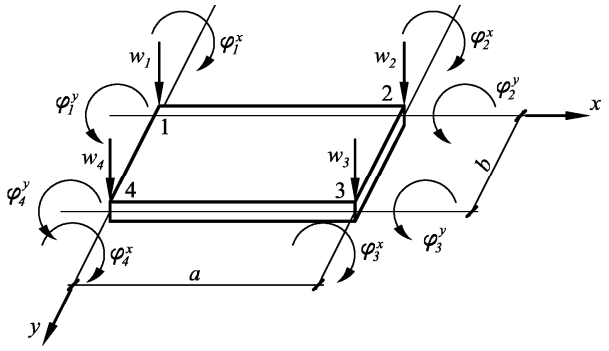

Fig. 2. Finite element used

The work of external forces is calculated as follows:

$$W = -\int_A p(x,y)\,w(x,y)\,dA. \qquad (24)$$

The following approximation is adopted for the deflection:

$$w = f_1 + f_2 x + f_3 y + f_4 x^2 + f_5 y^2 + f_6 xy + f_7 x^2 y + f_8 xy^2 + f_9 x^3 + f_{10} y^3 + f_{11} x^3 y + f_{12} xy^3 = [\Psi]\{f\}, \qquad (25)$$

where

$$\{f\}^{\mathrm{T}} = \{f_1\ f_2\ f_3\ f_4\ f_5\ f_6\ f_7\ f_8\ f_9\ f_{10}\ f_{11}\ f_{12}\};$$

$$[\Psi] = \{1\ x\ y\ x^2\ y^2\ xy\ x^2 y\ xy^2\ x^3\ y^3\ x^3 y\ xy^3\}.$$

The displacement field of the element can be written as:

$$\{w\ \ \varphi_x\ \ \varphi_y\}^T = \left\{w\ \ \frac{\partial w}{\partial x}\ \ \frac{\partial w}{\partial y}\right\}^T =$$

$$= \begin{bmatrix} 1 & x & y & x^2 & y^2 & xy & x^2 y & xy^2 & x^3 & y^3 & x^3 y & xy^3 \\ 0 & 1 & 0 & 2x & 0 & y & 2xy & y^2 & 3x^2 & 0 & 3x^2 y & y^3 \\ 0 & 0 & 1 & 0 & 2y & x & x^2 & 2xy & 0 & 3y^2 & x^3 & 3y^2 x \end{bmatrix} \{f\}. \qquad (26)$$

The vector of polynomial coefficients $\{f\}$ is determined by substituting the nodal coordinates into (26):

$$\{U^e\} = [C]\cdot\{f\} \rightarrow \{f\} = [C]^{-1}\{U^e\}, \qquad (27)$$

where

$$\{U^e\} = \{w_1\ \ \varphi_1^x\ \ \varphi_1^y\ \ w_2\ \ \varphi_2^x\ \ \varphi_2^y\ \ w_3\ \ \varphi_3^x\ \ \varphi_3^y\ \ w_4\ \ \varphi_4^x\ \ \varphi_4^y\}^T$$

is the vector of nodal displacements of the element,

$$[C] = \begin{bmatrix} 1 & 0 & 0 & 0 & 0 & 0 & 0 & 0 & 0 & 0 & 0 & 0 \\ 0 & 1 & 0 & 0 & 0 & 0 & 0 & 0 & 0 & 0 & 0 & 0 \\ 0 & 0 & 1 & 0 & 0 & 0 & 0 & 0 & 0 & 0 & 0 & 0 \\ 1 & a & 0 & a^2 & 0 & 0 & 0 & 0 & a^3 & 0 & 0 & 0 \\ 0 & 1 & 0 & 2a & 0 & 0 & 0 & 0 & 3a^2 & 0 & 0 & 0 \\ 0 & 0 & 1 & 0 & 0 & a & a^2 & 0 & 0 & 0 & a^3 & 0 \\ 1 & a & b & a^2 & b^2 & ab & a^2 b & ab^2 & a^3 & b^3 & a^3 b & ab^3 \\ 0 & 1 & 0 & 2a & 0 & b & 2ab & b^2 & 3a^2 & 0 & 3a^2 b & b^3 \\ 0 & 0 & 1 & 0 & 2b & a & a^2 & 2ab & 0 & 3b^2 & a^3 & 3ab^2 \\ 1 & 0 & b & 0 & b^2 & 0 & 0 & 0 & 0 & b^3 & 0 & 0 \\ 0 & 1 & 0 & 0 & 0 & b & 0 & b^2 & 0 & 0 & 0 & b^3 \\ 0 & 0 & 1 & 0 & 2b & 0 & 0 & 0 & 0 & 3b^2 & 0 & 0 \end{bmatrix}$$

The curvature vector can be written as:

$$\{\kappa\} = \begin{Bmatrix} \chi_x \\ \chi_y \\ 2\chi_{xy} \end{Bmatrix} = \begin{Bmatrix} \dfrac{\partial^2 w}{\partial x^2} \\ \dfrac{\partial^2 w}{\partial y^2} \\ 2\dfrac{\partial^2 w}{\partial x \partial y} \end{Bmatrix} =$$

$$= \begin{bmatrix} 0 & 0 & 0 & 2 & 0 & 0 & 2y & 0 & 6x & 0 & 6xy & 0 \\ 0 & 0 & 0 & 0 & 2 & 0 & 0 & 2x & 0 & 6y & 0 & 6xy \\ 0 & 0 & 0 & 0 & 0 & 2 & 4x & 4y & 0 & 0 & 6x^2 & 6y^2 \end{bmatrix} \{f\} =$$

$$= \begin{bmatrix} 0 & 0 & 0 & 2 & 0 & 0 & 2y & 0 & 6x & 0 & 6xy & 0 \\ 0 & 0 & 0 & 0 & 2 & 0 & 0 & 2x & 0 & 6y & 0 & 6xy \\ 0 & 0 & 0 & 0 & 0 & 2 & 4x & 4y & 0 & 0 & 6x^2 & 6y^2 \end{bmatrix} \times$$

$$\times [C]^{-1}\{U^e\} = [B]\{U^e\}. \qquad (28)$$

Substituting (28) into (20) yields the following expression for the potential strain energy of the element:

$$\Pi^e = \frac{1}{2}\{U^e\}^T \int_A [B]^T [D][B]\,dA\{U^e\} + \{U^e\}^T \int_A [B]^T\,dA\cdot\{M^*\} =$$

$$= \frac{1}{2}\{U^e\}^T [K^e]\{U^e\} - \{U^e\}^T \{F^{e*}\}, \qquad (29)$$

where $[K^e] = \int_A [B]^T [D][B]\,dA$ is the stiffness matrix of the finite element,

$\{F^{e*}\} = -\int_A [B]^T\,dA\cdot\{M^*\}$ is the contribution of thermal and shrinkage strains to the load vector.

To express the work of external forces, the Laplacian differential operator applied to the deflection can be written as follows:

$$\nabla^2 w = \frac{1}{2}\nabla^2\left([\Psi][C^{-1}]\{U^e\}\right) + \frac{1}{2}\nabla^2\left([\Psi][C^{-1}]\{U^e\}\right) =$$

$$= \frac{1}{2}\nabla^2\left([\Psi][C^{-1}]\{U^e\}\right) + \frac{1}{2}\nabla^2\left([\Psi][C^{-1}]\{U^e\}\right)^T =$$

$$= \frac{1}{2}\nabla^2([\Psi])[C^{-1}]\{U^e\} + \frac{1}{2}\{U^e\}^T [C^{-1}]^T \nabla^2\left([\Psi]^T\right). \qquad (30)$$

This representation is used in order to obtain symmetric matrices.

As a result, the work of external forces for a single FE can be written in the following form:

$$W^e = -\{U^e\}^T [C^{-1}]^T \int_A ([\Psi]^T \cdot C_1 \cdot [\Psi] -$$

$$-C_2\left([\Psi]^T \frac{1}{2}\nabla^2([\Psi]) + \frac{1}{2}\nabla^2\left([\Psi]^T\right)[\Psi]\right))dA[C^{-1}]\{U^e\} =$$

$$= -\{U^e\}^T [K_s^e]\{U^e\}, \qquad (31)$$

where $\left[K_s^e\right]$ is the additional term in the stiffness matrix accounting for the contribution of the elastic base.

Based on (29) and (31), the Lagrange functional for the entire slab takes the following form:

$$\Lambda = \frac{1}{2}\{U\}^T\left(\left[K\right]+\left[K_s\right]\right)\{U\}-\{U\}^T\left\{F^*\right\}, \quad (32)$$

where $\left[K\right]=\sum[K^e]$ is the stiffness matrix of the entire slab, $\left[K_s\right]=\sum[K_s^e]$ is the contribution of the elastic base to the stiffness matrix, $\left\{F^*\right\}=\sum\left\{F^{e*}\right\}$ is the load vector.

The system of FEM equations can be obtained by minimizing the Lagrange functional with respect to the nodal displacement vector:

$$\frac{\partial\Lambda}{\partial\{U\}}=0\rightarrow\left(\left[K\right]+\left[K_s\right]\right)\{U\}=\left\{F^*\right\}. \quad (33)$$

The calculation of thermal stresses is carried out in an uncoupled quasi-static formulation; i.e., it is assumed that the stress state does not affect the temperature field. The calculation of temperature fields is performed using the finite element method in a one-dimensional formulation according to the procedure presented in (Chepurnenko et al., 2022a).

Results and Discussion

Validation of the developed method was performed using the experimental data and numerical simulation results presented in (Smolana et al., 2022). The initial data for the analysis are given in Table 1.

The slab reinforcement consisted of two layers of reinforcement placed at the upper and lower surfaces, with a concrete cover of 6 cm. The diameter of the reinforcing bars was 25 mm, with a spacing of 15 cm.

The measured ambient temperature variation at the construction site is shown in Fig. 3.

The dependence of the concrete elastic modulus on time was taken as a function of the equivalent age t_{eq} in accordance with the study carried out by Smolana et al. (2022):

$$E(t)=E\left(t_{eq}\right)=\alpha_1 e^{-\left(\frac{\tau_1}{t_{eq}}\right)^{\beta_1}}+\alpha_2 e^{-\left(\frac{\tau_2}{t_{eq}}\right)^{\beta_2}}, \quad (34)$$

where α_1 = 15 GPa, α_2 = 20 GPa, τ_1 = 2 days, τ_2 = 4 days, $\beta_1=\beta_2=1.5$.

The equivalent age of concrete is determined by the integral:

$$t_{eq}=\int_0^t e^{-\frac{E_a}{R}\left(\frac{1}{T(\tau)}-\frac{1}{T_{ref}}\right)}d\tau, \quad (35)$$

where $T(\tau)$ is the concrete temperature at time τ in Kelvins, T_{ref} = 293 K, $R=8.314$ J/(mol·K) is the universal gas constant, $E_a=38500$ J/mol is the activation energy.

Since Smolana et al. (2022) did not provide sufficient data on the heat release of concrete, the heat release function was adopted based on studies performed by Nesvetaev et al. (2024) and Nesvetaev and Koryanova (2023):

$$Q(t)=Q_{28}\cdot\exp\left[k\cdot\left(1-\left(\frac{28}{t}\right)^x\right)\right], \quad (36)$$

Table 1. **Initial data for the analysis**

Quantity	Designation	Units of measurement	Value
Foundation slab thickness	h	m	2.1
Foundation slab width	a	m	26.5
Foundation slab length	b	m	41.5
Soil mass thickness	H	m	10
Heat transfer coefficient on the upper surface of the slab	h_{up}	W/(m²·°C)	30
Initial temperature of the concrete mixture	T_0	°C	24
Initial temperature of the soil mass	T_g	°C	16
Concrete density	ρ_b	kg/m³	2,349
Soil density	ρ_g	kg/m³	2,070
Thermal conductivity coefficient of concrete	λ_b	W/(m·°C)	2.67
Thermal conductivity coefficient of soil	λ_g	W/(m·°C)	1.4
Specific heat capacity of concrete	c_b	J/(kg·°C)	1,000
Specific heat capacity of soil	c_g	J/(kg·T)	1,039
Coefficient of linear thermal expansion of concrete	α	1/°C	$1.2\cdot10^{-5}$
Poisson's ratio of concrete	ν	–	0.2
Poisson's ratio of soil	ν_g	–	0.2
Modulus of elasticity of soil	E_g	MPa	30
Modulus of elasticity of steel	E_s	MPa	$2.1\cdot10^5$

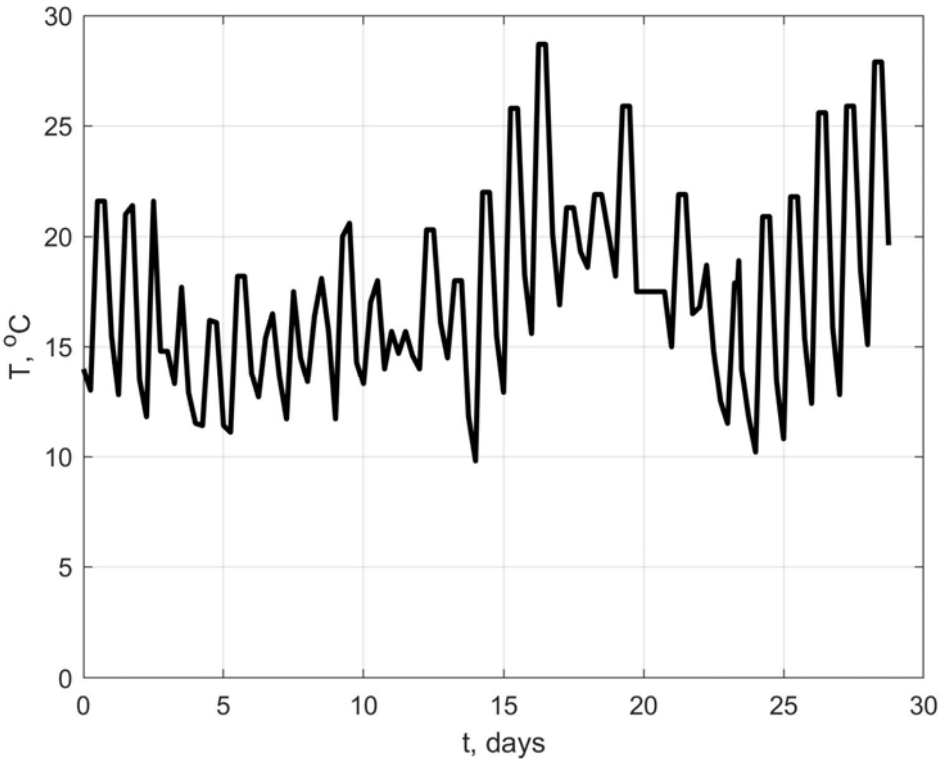

Fig. 3. Ambient temperature variation over time

where t is time in days, Q_{28} is the amount of heat released during the first 28 days of hardening, MJ/m^3, k and x are coefficients characterizing the kinetics of concrete hardening.

The parameters Q_{28}, k and x were selected in such a way as to ensure the best possible correspondence between the experimental temperature–time curves and the numerical predictions. To select the parameters Q_{28}, k and x, the nonlinear optimization package MATLAB Optimization Toolbox was used. An objective function $f(Q_{28},k,x)$ was implemented to calculate the sum of squared deviations between the theoretical and experimental temperature values. As a result of minimizing the objective function using the interior point method (Byrd et al., 1999), the following values were obtained: Q_{28} = 51.7 MJ/m^3, k = 1.62·10^{-5}, x = 3.76. Fig. 4 presents the experimental curves (dashed lines) together with the theoretical curves (solid lines) of temperature evolution in time at the center of the foundation slab — both at mid-depth (shown in green) and near the bottom surface (shown in red). For the mid-depth point, the agreement of results is very good, while for the point near the bottom surface it is satisfactory.

Fig. 5 shows the time-dependent variation of the stresses σ_x at the center of the foundation slab at mid-depth. The red curve corresponds to the experimental results, the yellow curve corresponds to the results of finite element analysis, obtained in a three-dimensional formulation, in the work by Smolana et al. (2022). The blue curve shows the solution obtained using the authors' approach The blue dashed line represents the solution obtained using the authors' method in the absence of reinforcement. From Fig. 5 it can be seen that, up to approximately seven days, the discrepancy between the results obtained by the authors' method and those of the finite element modeling is insignificant. The subsequent divergence can be explained by the fact that it was not possible to achieve a perfect match between the calculated and experimental temperatures due to the lack of detailed data on the heat release of concrete.

The deviation between the calculated stresses and the experimental results can also be attributed not only to insufficient information on the heat release of concrete, but also to the presence of shrinkage and creep in concrete, as well as differences between the actual time-dependent modulus of elasticity and the curve described by Eq. (34). A notable feature is the nearly instantaneous drop of the experimental stress curve to zero at t = 16 days, which is likely associated either with sensor failure or the formation of a crack.

As can also be seen from Fig. 5, the reinforcement of the slab in the considered example does not have a noticeable effect on the stress–strain state. This can be explained by the relatively low reinforcement ratio, as well as by the fact that, following Smolana et al. (2022), the coefficient of linear thermal expansion of concrete was taken equal to that of steel. Depending on the

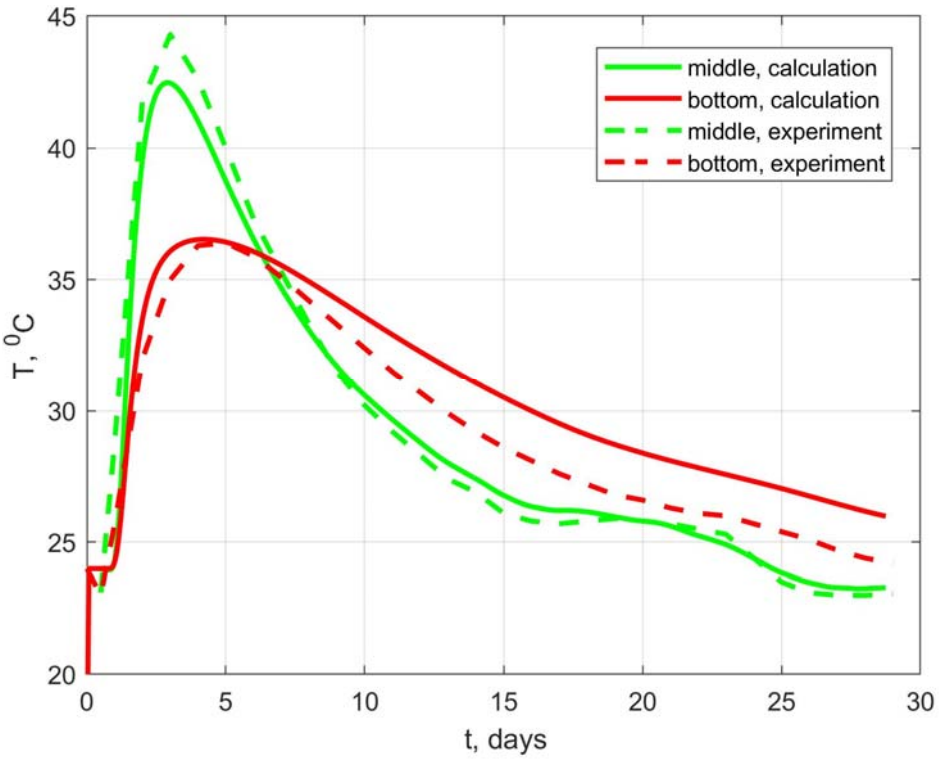

Fig. 4. Experimental and theoretical temperature–time curves

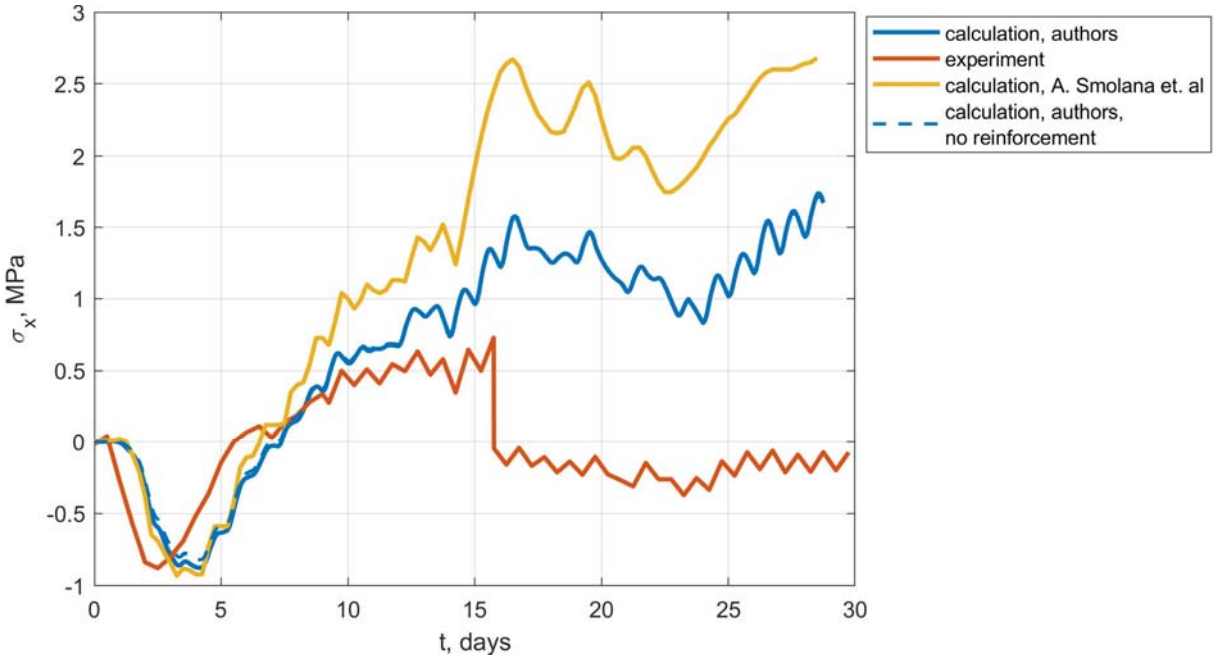

Fig. 5. Time-dependent variation of the stresses at the center of the foundation slab at mid-depth

concrete composition, the coefficient of linear thermal expansion varies from 5.4 to 14.4 · 10^{-6} 1/°C (Naik et al., 2011). The value most commonly used in calculations is 10^{-5} 1/ °C (Mackiewicz and Szydło, 2020).

Fig. 6 presents the results of the stress analysis for different values of the coefficient of linear thermal expansion of concrete and the reinforcement ratio $\mu = \mu_x = \mu_y$. The reinforcement ratio was defined as the ratio of the total area of reinforcing bars along one axis per running meter of the slab length to its thickness, expressed as a percentage:

$$\mu_x = \frac{\sum_{i=1}^{n_x} A_{sx,i}}{h} 100\%;\ \mu_y = \frac{\sum_{i=1}^{n_y} A_{sy,i}}{h} 100\%. \quad (37)$$

From Fig. 6, it is evident that the maximum tensile stresses increase with both the reinforcement

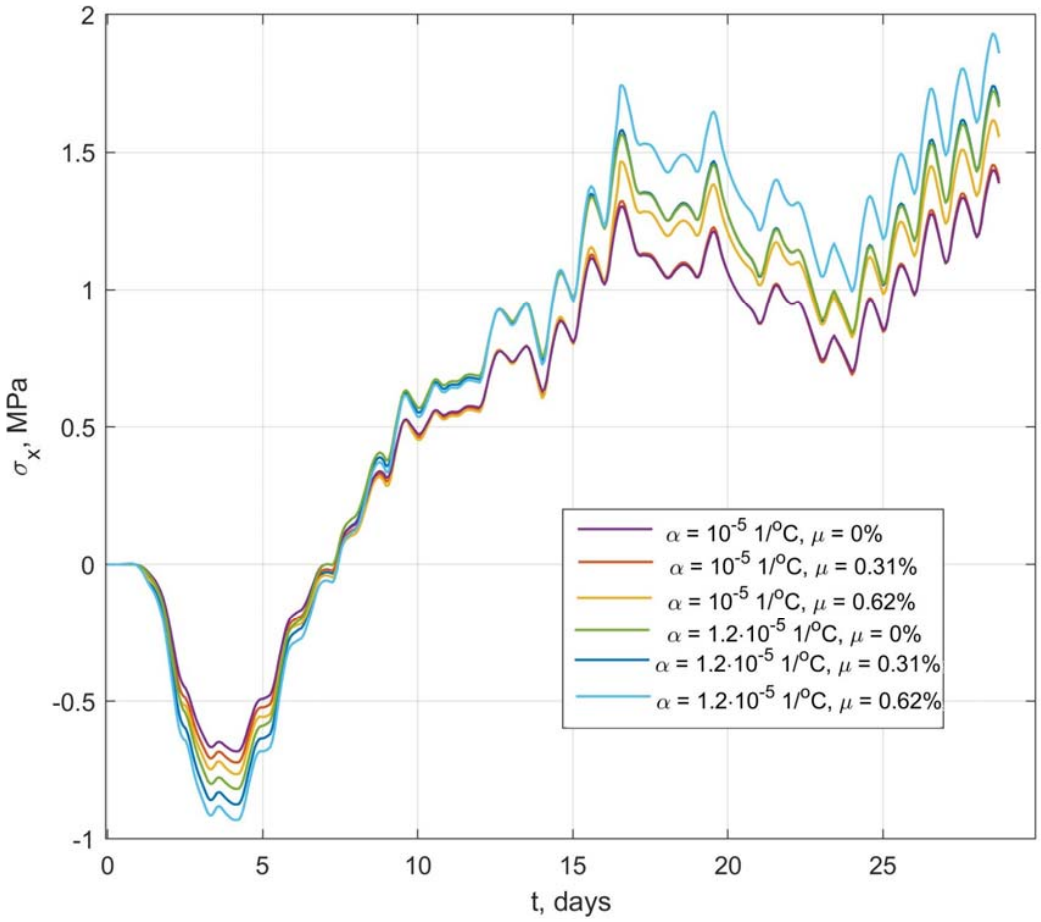

Fig. 6. Stress analysis results for various values of the coefficient of linear thermal expansion and reinforcement ratio

ratio and the coefficient of linear thermal expansion of concrete.

Conclusions

1. A simplified method was proposed for determining the stress–strain state during the construction of monolithic foundation slabs while accounting for the foundation bed compliance. The foundation bed was modeled using the Pasternak model with two foundation moduli. The proposed method reduces the three-dimensional problem of thermal stress analysis to a two-dimensional one based on the assumption of linear strain distribution through the slab thickness.

2. The proposed method was verified against experimental data as well as against the results of three-dimensional finite element modeling reported in (Smolana et al., 2022). The agreement between the results obtained using the present method and the experimental data is no worse than that demonstrated in the referenced study, despite the reduced dimensionality of the problem. Up to 10 days, the discrepancy between the experimental maximum tensile stresses and those calculated using the proposed method does not exceed 5 %.

3. A parametric study was carried out to investigate the influence of the coefficient of linear thermal expansion of concrete and the reinforcement ratio on the magnitude of thermal stresses. It was established that increasing both the reinforcement ratio and the coefficient of linear thermal expansion leads to higher maximum tensile stresses.

4. The model developed in this study allows the incorporation of concrete shrinkage; however, shrinkage was not considered in the experiment modeling due to the lack of sufficient data. Concrete creep was also not included in the analysis. In future research, we plan to examine the influence of these two factors on the stress–strain state.

5. The deformation model developed in this work enables prediction of crack initiation, but not the subsequent crack propagation or crack width development. To track the evolution of the stress–strain state after crack formation, it is necessary to account for the material nonlinearity of concrete, which also represents a direction for further research.

Funding

This research was supported by Russian Science Foundation grant No. 25-19-00164, https://rscf.ru/project/25-19-00164/.

References

Buffo-Lacarrière, L., Sellier, A., Turatsinze, A., and Escadeillas, G. (2011). Finite element modelling of hardening concrete: application to the prediction of early age cracking for massive reinforced structures. *Materials and Structures*, Vol. 44, Issue 10, pp. 1821–1835. DOI: 10.1617/s11527-011-9740-y.

Bushmanova, A. V., Barabanschikov, Yu. G., Semenov, K. V., Struchkova, A. Ya., and Manovitsky, S. S. (2017). Thermal cracking resistance in massive foundation slabs in the building period. *Magazine of Civil Engineering*, Issue 8 (76), pp. 193–200. DOI: 10.18720/MCE.76.17.

Byrd, R. H., Hribar, M. E., and Nocedal, J. (1999). An interior point algorithm for large-scale nonlinear programming. *SIAM Journal on Optimization*, Vol. 9, Issue 4, pp. 877–900. DOI: 10.1137/S1052623497325107.

Cajka, R., Marcalikova, Z., Bilek, V., and Sucharda, O. (2020). Numerical modeling and analysis of concrete slabs in interaction with subsoil. *Sustainability*, Vol. 12, Issue 23, 9868. DOI: 10.3390/su12239868.

Chepurnenko, A., Nesvetaev, G., and Koryanova, Yu. (2022a). Modeling non-stationary temperature fields when constructing mass cast-in-situ reinforced-concrete foundation slabs. *Architecture and Engineering*, Vol. 7, Issue 2, pp. 66–78. DOI: 10.23968/2500-0055-2022-7-2-66-78.

Chepurnenko, A., Nesvetaev, G., Koryanova, Yu., and Yazyev, B. (2022b). Simplified model for determining the stress-strain state in massive monolithic foundation slabs during construction. *International Journal for Computational Civil and Structural Engineering*, Vol. 18, No. 3, pp. 126–136. DOI: 10.22337/2587-9618-2022-18-3-126-136.

Chepurnenko, A., Turina, V., and Akopyan, V. (2024). Determination of temperature stresses during the construction of massive monolithic foundation slabs, taking into account the subgrade compliance. *The Open Civil Engineering Journal*, Vol. 18, e18741495321409. DOI: 10.2174/0118741495321409240527051344.

Chuc, N. T., Le Quy Don, Thoan, P. V., and Kiet, B. A. (2018). The effects of insulation thickness on temperature field and evaluating cracking in the mass concrete. *Electronic Journal of Structural Engineering*, Vol. 18, No. 2, pp. 128–132. DOI: 10.56748/ejse.182722.

Egorova, E. S., Ioskevich, A. V., Ioskevich, V. V., Agishev, K. N., and Kozhevnikov, V. Yu. (2016). Soil model implemented in the software packages SCAD Office and Plaxis 3D. *Construction of Unique Buildings and Structures*, No. 3 (42), pp. 31–60.

Gatiev, M. Sh., Ayubov, N. A., Klyuev, S. V., and Litvinov, S. V. (2023). Influence of shear deformations on the stress-strain state of reinforced concrete slabs. *System Technologies*, No. 4 (49), pp. 100–108. DOI: 10.55287/22275398_2023_4_100.

Havlásek, P., Šmilauer, V., Hájková, K., and Baquerizo, L. (2017). Thermo-mechanical simulations of early-age concrete cracking with durability predictions. *IOP Conference Series: Materials Science and Engineering*, Vol. 236, 012052. DOI: 10.1088/1757-899X/236/1/012052.

Johansson, H. and Heinegård, M. (2020). *Reinforced concrete structures subjected to imposed deformations: a study of cracking due to shrinkage in slab foundations for residential houses*. [online] Available at: https://lup.lub.lu.se/luur/download?func=downloadFile&recordOId=9017916&fileOId=9017917 [Date accessed 02.12.2025].

Klemczak, B. and Knoppik-Wróbel, A. (2011). Early age thermal and shrinkage cracks in concrete structures–description of the problem. *Architecture, Civil Engineering, Environment*, Vol. 4, Issue 2, pp. 35–48.

Korotchenko, I., Ivanov, E., Semenov, K., and Barabanshchikov, Yu. (2016). Thermal stressed state in massive concrete structures in the winter building period. *MATEC Web of Conferences*, Vol. 53, 01001. DOI: 10.1051/matecconf/20165301001.

Kuriakose, B., Nageswara Rao, B., and Dodagoudar, G. R. (2016). Early-age temperature distribution in a massive concrete foundation. *Procedia Technology*, Vol. 25, pp. 107–114. DOI: 10.1016/j.protcy.2016.08.087.

Liu, Y. and Schindler, A. K. (2020). Finite-element modeling of early-age concrete stress development. *Journal of Materials in Civil Engineering*, Vol. 32, Issue 1, 04019338. DOI: 10.1061/(ASCE)MT.1943-5533.0002988.

Mackiewicz, P. and Szydło, A. (2020). Thermal stress analysis in concrete pavements. *Journal of Transportation Engineering, Part B: Pavements*, Vol. 146, Issue 3, 06020002. DOI: 10.1061/JPEODX.0000192.

Mathern, A. and Yang, J. (2021). A practical finite element modeling strategy to capture cracking and crushing behavior of reinforced concrete structures. *Materials*, Vol. 14, Issue 3, 506. DOI: 10.3390/ma14030506.

Naik, T. R., Kraus, R. N., and Kumar, R. (2011). Influence of types of coarse aggregates on the coefficient of thermal expansion of concrete. *Journal of Materials in Civil Engineering*, Vol. 23, Issue 4, pp. 467–472. DOI: 10.1061/(ASCE)MT.1943-5533.0000198.

Nama, P., Jain, A., Srivastava, R., and Bhatia, Y. (2015). Study on causes of cracks & its preventive measures in concrete structures. *International Journal of Engineering Research and Applications*, Vol. 5, Issue 5, pp. 119–123.

Nesvetaev, G. V. and Koryanova, Yu. I. (2023). Forecasting the strength gaining kinetics of the concrete hardening in the abnormal conditions. *Modern Trends in Construction, Urban Planning and Territorial Planning*, Vol. 2, No. 4, pp. 59–68. DOI: 10.23947/2949-1835-2023-2-4-59-68.

Nesvetaev, G. V., Koryanova, Yu. I., and Shut, V. V. (2024). Specific heat dissipation of concrete and the risk of early cracking of massive reinforced concrete foundation slabs. *Construction Materials and Products*, Vol. 7, No. 4, 3. DOI: 10.58224/2618-7183-2024-7-4-3.

Petrov, V. V. (2018). *Theory of plate and shell analysis*. Moscow: Publishing House of the Association of Construction Universities (ASV), 410 p.

Safiuddin, M., Amrul Kaish, A. B. M., Woon, C.-O., and Raman, S. N. (2018). Early-age cracking in concrete: causes, consequences, remedial measures, and recommendations. *Applied Sciences*, Vol. 8, Issue 10, 1730. DOI: 10.3390/app8101730.

Slowik, V., Neumann, A., Dorow, J., and Schmidt, M. (2008). Early age cracking and its influence on the durability of concrete structures. In: Tanabe, T., Sakata, K., Mihashi, H., Sato, R., Maekawa, K., and Nakamura, H. (eds.). *Proceedings of the 8th International Conference on Creep, Shrinkage and Durability Mechanics of Concrete and Concrete Structures*, Vol. 2. Boca Raton: CRC Press, pp. 471–477. DOI: 10.1201/9780203882955.ch62.

Smolana, A., Klemczak, B., Azenha, M., and Schlicke, D. (2022). Thermo-mechanical analysis of mass concrete foundation slabs at early age—essential aspects and experiences from the FE modelling. *Materials*, Vol. 15, Issue 5, 1815. DOI: 10.3390/ma15051815.

Wang, Q., Ren, X., and Ballarini, R. (2020). A multifield model for early-age massive concrete structures: hydration, damage, and creep. *Journal of Engineering Mechanics*, Vol. 146, Issue 10, 04020115. DOI: 10.1061/(ASCE)EM.1943-7889.0001851.

ИНЖЕНЕРНЫЙ МЕТОД ДЛЯ ОПРЕДЕЛЕНИЯ ТЕМПЕРАТУРНЫХ НАПРЯЖЕНИЙ ПРИ ВОЗВЕДЕНИИ ФУНДАМЕНТНЫХ ПЛИТ С УЧЕТОМ ПОДАТЛИВОСТИ ОСНОВАНИЯ

Василина Сергеевна Тюрина, Антон Сергеевич Чепурненко*, Владимир Феликсович Акопян

Донской государственный технический университет, Ростов-на-Дону, Россия

*E-mail: anton_chepurnenk@mail.ru

Аннотация

Введение. Для массивных монолитных фундаментных плит актуальна проблема раннего трещинообразования, обусловленного экзотермией бетона при твердении. Выбор оптимальных путей решения этой проблемы может быть осуществлен на основе компьютерного моделирования. **Целью работы** является разработка упрощенной конечно-элементной модели для определения напряженно-деформированного состояния фундаментных плит в процессе возведения с учетом податливости основания и ее апробация на существующих экспериментальных данных, а также результатах расчета других авторов. **Использованы следующие методы**: конечно-элементное моделирование пластинчатыми конечными элементами в среде MATLAB с использованием разработанного авторами программного обеспечения, сводящего трехмерную задачу определения напряженно-деформированного состояния к двумерной. В качестве модели грунтового основания использована модель Пастернака с двумя коэффициентами постели. **В результате** установлено, что решение авторов хорошо согласуется с результатами численного моделирования, полученными другими авторами в трехмерной постановке. Также получено удовлетворительное совпадение с результатами эксперимента. Проведено исследование влияния коэффициента армирования и коэффициента линейного температурного расширения бетона на напряженно-деформированное состояние.

Ключевые слова: массивные железобетонные конструкции; фундаментная плита; трещинообразование; температурные напряжения; метод конечных элементов; коэффициент постели.